

Excitonic splitting and vibronic coupling in 1,2-diphenoxyethane: Conformation-specific effects in the weak coupling limit

Evan G. Buchanan, Patrick S. Walsh, David F. Plusquellic, and Timothy S. Zwier

Citation: *The Journal of Chemical Physics* **138**, 204313 (2013); doi: 10.1063/1.4807300

View online: <http://dx.doi.org/10.1063/1.4807300>

View Table of Contents: <http://scitation.aip.org/content/aip/journal/jcp/138/20?ver=pdfcov>

Published by the [AIP Publishing](#)

Articles you may be interested in

[Analysis of the S₂←S₀ vibronic spectrum of the ortho-cyanophenol dimer using a multimode vibronic coupling approach](#)

J. Chem. Phys. **142**, 084308 (2015); 10.1063/1.4913363

[Assessment of mode-mixing and Herzberg-Teller effects on two-photon absorption and resonance hyper-Raman spectra from a time-dependent approach](#)

J. Chem. Phys. **140**, 094107 (2014); 10.1063/1.4867273

[Excitonic splitting and coherent electronic energy transfer in the gas-phase benzoic acid dimer](#)

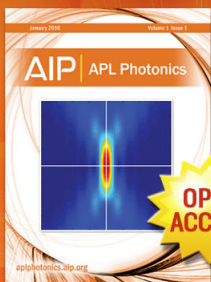
J. Chem. Phys. **137**, 204303 (2012); 10.1063/1.4767400

[The S₁/S₂ exciton interaction in 2-pyridone-6-methyl-2-pyridone: Davydov splitting, vibronic coupling, and vibronic quenching](#)

J. Chem. Phys. **135**, 154311 (2011); 10.1063/1.3652759

[Single vibronic level emission spectroscopic studies of the ground state energy levels and molecular structures of jet-cooled HGeBr, DGeBr, HGeI, and DGeI](#)

J. Chem. Phys. **125**, 114301 (2006); 10.1063/1.2355496



Launching in 2016!

The future of applied photonics research is here

OPEN
ACCESS

AIP | APL
Photonics

Excitonic splitting and vibronic coupling in 1,2-diphenoxyethane: Conformation-specific effects in the weak coupling limit

Evan G. Buchanan,¹ Patrick S. Walsh,¹ David F. Plusquellic,^{2,a)} and Timothy S. Zwier^{1,a)}

¹Department of Chemistry, Purdue University, West Lafayette, Indiana 47907-2084 USA

²Quantum Electronics and Photonics Division, Physical Measurement Laboratory, National Institute of Standards and Technology, Boulder, Colorado 80305-3328, USA

(Received 19 March 2013; accepted 2 May 2013; published online 30 May 2013)

Vibrationally and rotationally resolved electronic spectra of 1,2-diphenoxyethane ($C_6H_5-O-CH_2-CH_2-O-C_6H_5$, DPOE) are reported for the isolated molecule under jet-cooled conditions. The spectra demonstrate that the two excited surfaces are within a few cm^{-1} of one another over significant regions of the torsional potential energy surfaces that modulate the position and orientation of the two aromatic rings with respect to one another. Two-color resonant two-photon ionization (2C-R2PI) and laser-induced fluorescence excitation spectra were recorded in the near-ultraviolet in the region of the close-lying S_0-S_1 and S_0-S_2 states ($36\,400-36\,750\text{ cm}^{-1}$). In previous work, double resonance spectroscopy in the ultraviolet and alkyl CH stretch regions of the infrared was used to identify and assign transitions to two conformational isomers differing primarily in the central C-C dihedral angle, a *tgt* conformation with C_2 symmetry and a *ttt* conformation with C_{2h} symmetry [E. G. Buchanan, E. L. Sibert, and T. S. Zwier, *J. Phys. Chem. A* **117**, 2800 (2013)]. Comparison of 2C-R2PI spectra recorded in the m/z 214 (all ^{12}C) and m/z 215 (one ^{13}C) mass channels demonstrate the close proximity of the S_1 and S_2 excited states for both conformations, with an upper bound of 4 cm^{-1} between them. High resolution spectra of the origin band of the *tgt* conformer reveal it to consist of two transitions at $36\,422.91$ and $36\,423.93\text{ cm}^{-1}$, with transition dipole moments perpendicular to one another. These are assigned to the S_0-S_1 and S_0-S_2 origin transitions with excited states of A and B symmetry, respectively, and an excitonic splitting of only 1.02 cm^{-1} . The excited state rotational constants and transition dipole coupling model directions prove that the electronic excitation is delocalized over the two rings. The *ttt* conformer has only one dipole-allowed electronic transition ($A_g \rightarrow B_u$) giving rise to a pure b-type band at $36\,508.77\text{ cm}^{-1}$. Here, the asymmetry induced by a single ^{13}C atom in one of the rings is sufficient to localize the electronic excitation in one or the other ring. Dispersed fluorescence (DFL) spectra are used to provide assignments for all vibronic structure in the first 200 cm^{-1} of both conformers. In the *tgt* conformer, both “a” and “b” symmetry fundamentals are observed, consistent with extensive vibronic coupling between the two dipole-allowed, nearly degenerate excited states. In the *ttt* conformer, the lowest frequency vibronic transition located 46 cm^{-1} above the B_u origin is assigned to a b_u fundamental (labeled \bar{R}) built off the dipole-forbidden A_g state origin. The DFL spectrum of the $A_g(\bar{R}^1)$ level contains strong transitions to $v''(\bar{R}) = 0, 1,$ and 2 , seemingly at odds with vibronic coupling models. Studies of the DFL spectrum of this band as a function of distance from the nozzle reveal that much of the intensity in $v'' = 1$ arises from collisions of DPOE while in the excited state $A_g(v_b' = 1)$ level with He, producing $B_u(\bar{R} = 1)$ levels with large collision cross section. The remaining intensity in the fundamental at large x/D is ascribed to emission from the ^{13}C isotopomer, for which this emission is dipole-allowed.
 © 2013 AIP Publishing LLC. [<http://dx.doi.org/10.1063/1.4807300>]

I. INTRODUCTION

Excitonic and vibronic coupling between electronic chromophores plays an essential role in the absorption/emission properties and excited state dynamics of molecular samples with important applications, including light-harvesting complexes,¹⁻⁴ chromophore arrays (e.g., J- and H-aggregates),^{5,6} conjugated polymers,⁷⁻⁹ and fluorescence resonance energy transfer (FRET).¹⁰ This interest is fueled

in part by new experimental methods such as 2D-electronic spectroscopy,^{11,12} which are providing new insight to the femtosecond dynamics of electronic energy transfer. Among the issues under active investigation is the possible role played by electronic coherence in directing electronic energy transfer through an array of chromophores, and the extent to which vibrational motions are involved.^{13,14}

Regardless of the circumstance, the structural and dynamical consequences of electronic near-degeneracy provide a particular challenge to modern theories seeking to understand them. While many of these applications involve multiple chromophores in a complex environment at room

^{a)}Authors to whom correspondence should be addressed. Electronic addresses: david.plusquellic@nist.gov and Zwier@purdue.edu

temperature, one useful strategy is to seek to control or remove many of the complicating factors in order to focus attention on the fundamental aspects of interchromophore coupling. To that end, laser spectroscopy of the gas-phase bichromophore cooled in a supersonic jet provides exquisite details of the vibronic coupling on a single-vibronic level basis free from the interference from solvent.^{15–22} When the two chromophores are incorporated into separate molecules, the supersonic expansion serves as a means for synthesizing the molecular dimer and collapsing its population entirely into the ground state vibrational zero-point level.^{15–23}

The other circumstance in which multiple chromophores exist in close proximity is when they are incorporated as part of the same molecule. Model bichromophores can either be held rigidly in a framework which defines the interchromophore separation and orientation,^{24,25} or as part of a flexible linker along which the interchromophore distance and orientation may vary.^{26–38} Flexible linkages offer the tantalizing prospect of studying interchromophore vibronic coupling on a conformation-specific basis under jet-cooled conditions in which population is collisionally cooled into more than one conformational zero-point level. The uncoupled excited state energies and interchromophore electronic coupling will be modulated from one conformer to the next by changes in the distance and relative orientation of the chromophores, and the nature of the vibrational motions involved.

Model flexible bichromophores can either incorporate two identical monomers,^{28–35} or consist of chemically distinct donor and acceptor sub-units.^{39,40} In a few cases, conformation-specific data have shed light on the way in which the ground state conformation of the molecule dictates the excited state spectroscopy and dynamics, producing conformation-selective broadening in the excitation spectrum, redshifted emission, or differing energy thresholds to exciplex formation.^{29,30,39}

Recent experiments and theory are shedding qualitative new light on the spectroscopic consequences of interchromophore coupling.^{16,18,19,41} Much of this work compares experiment with the predictions of a diabatic model of the vibronic coupling based on Förster theory,⁴² as developed by Fulton and Gouterman (FG)^{43,44} for the specific case of a bichromophore coupled by a single vibrational mode. Extension of this model to multiple vibrational modes^{34,41} and to asymmetric bichromophores⁴¹ have contributed to the growing ability to quantitatively account for the observed vibronic coupling patterns.

Recently, Leutwyler, Koppel, and co-workers^{16,45} have developed an adiabatic vibronic coupling model and used it to obtain a quantitatively accurate account of the observed excitonic splitting in 2-aminopyridine, *o*-cyanophenol, 2-pyridone, and benzoic acid dimers, all of which are in the weak coupling limit. The theory reproduces the experimental excitonic splitting determined by the diabatic model, but provides a more intuitive picture of the excitonic splitting in the weak coupling limit. Here, the electronic energy transfer occurs through a barrier on the adiabatic surface, with the excitonic splitting modeled as a tunneling splitting in which both nuclear distortions and interchromophore electronic energy transfer contribute to the tunneling rate.

In experiments to date on jet-cooled bichromophores, there are relatively few examples in which both the S_0 – S_1 and S_0 – S_2 transitions have been spectroscopically characterized. When the two chromophores are sufficiently different, fast electronic energy transfer between the two chromophores inhibits the identification of the lifetime broadened S_2 state. Furthermore, in cases where the two chromophores are identical and conformational symmetry exists, only one of the S_0 – S_1 or S_0 – S_2 transitions is often dipole-allowed.¹⁷ In several aromatic dimers, Leutwyler and co-workers^{18,19,16} have cleverly addressed this by breaking the symmetry through recording the spectrum of the singly ^{13}C substituted isotopomer in natural abundance using resonant two-photon ionization (R2PI) coupled with time-of-flight mass analysis.

Previous work from our group has focused attention on a series of prototypical flexible bichromophores that possess a single conformational isomer for diphenylmethane (DPM),^{33,35} and two isomers of both bis-(2-hydroxyphenyl)methane (2HDPM)³² and bis-(4-hydroxyphenyl)methane (b4HPM).³⁴ In these molecules, the spectroscopic consequences of internal mixing between the two excited electronic states have been characterized in some detail. In DPM, the excitonic splitting was determined to be 123 cm^{-1} , leading to a dual emission from the (nominal) S_2 origin that reported on its mixing with nearby vibrational levels built off the S_1 origin. This has stimulated theoretical developments that employ a multi-mode asymmetric vibronic coupling model as an extension of the theoretical framework developed by Fulton and Gouterman^{43,46} for symmetric bichromophores.⁴¹

A previous study reporting on the ground state conformational preferences of 1,2-diphenoxyethane ($\text{C}_6\text{H}_5\text{--O--CH}_2\text{--CH}_2\text{--O--C}_6\text{H}_5$, DPOE) provides the foundation for the present work,⁴⁷ which we briefly summarize here. A conformational search of the torsional potential energy surface for DPOE located 26 conformational minima. Two of the conformational isomers possessed an inversion center, while the remaining 12 structures are composed of pairs of non-superimposable mirror images with dihedral angles of opposite sign but identical magnitude. Experimentally, two conformational isomers were observed in the supersonic jet expansion and assigned based on infrared and vibronic data to the two lowest energy conformers of DPOE, with C_2 (*tg*) and C_{2h} (*ttt*) symmetry, as shown in Figure 1. Here, the central three dihedral angles are labeled as *trans* (*t*) or *gauche* (*g*). To establish the conformational assignments, calculated harmonic vibrational frequency were compared to the experimental alkyl CH stretch, CH bend, and CO stretch spectra. Using a reduced-dimension model, the Fermi resonances present in the alkyl CH stretch infrared spectrum were successfully modeled, confirming and strengthening the assignments based on the vibronic spectroscopy.

In the current paper, we provide a detailed spectroscopic characterization of the vibronic and rovibronic spectroscopy of DPOE in the region of the close-lying S_1 and S_2 state origins. High resolution ultraviolet spectra prove that the two dipole-allowed S_0 – S_1 and S_0 – S_2 origins of the *tg* isomer are separated by 1.02 cm^{-1} . Although the S_0 – S_1 origin of the *ttt* conformer is dipole-forbidden, 2C-R2PI spectra of the M+1

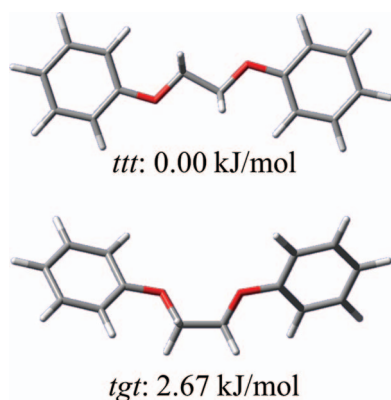


FIG. 1. Optimized structures for the two observed conformers of DPOE, with their relative energies calculated at the DFT M05-2X/6-31+G(d) level of theory.

mass channel for monomers possessing a single ^{13}C atom show a spectrum for the *ttt* conformer that possesses two dipole-allowed origins arising from near-complete localization of the electronic excitation in one or the other ring, with splitting of $\sim 4\text{ cm}^{-1}$. Thus, despite the seeming close proximity of the two chromophores, interchromophore coupling in DPOE is in the extreme limit of weak coupling. The results for DPOE thus provide a window on the spectroscopic consequences of vibronic coupling in this weak coupling limit in which the two electronic states are no more than a few cm^{-1} from one another over much of the torsional potential energy surface, with electronic excitation localized or delocalized by minute asymmetries in the local environment.

II. EXPERIMENTAL METHODS

Single and double-resonance techniques used to obtain the single-conformation ultraviolet and infrared spectra have been reported previously.⁴⁸ Details specific to the current work are briefly provided here. 1,2-diphenoxyethane (Aldrich) was heated to 90°C inside a stainless steel reservoir to obtain a sufficient vapor pressure. DPOE was seeded into a helium or neon buffer gas with a backing pressure of ~ 3 bars and passed through a pulsed valve with a $500\ \mu\text{m}$ orifice (Parker General Valve Series 9) to form the supersonic jet expansion.

Two-color resonant two-photon ionization (2C-R2PI) was employed to record the total electronic spectrum of all species present in the expansion. In 2C-R2PI, a 20 Hz UV laser resonantly excited DPOE to an excited state with a second lower-frequency, non-resonant 20 Hz UV laser used to ionize the molecules for detection with a multichannel plate.⁴⁹ Dispersed fluorescence (DFL) spectra were obtained in a fluorescence chamber described previously.⁵⁰ A $\frac{3}{4}$ -m monochromator with $50\ \mu\text{m}$ entrance slit provided DFL spectra with $\sim 9\text{ cm}^{-1}$ resolution. The dispersed emission was imaged onto the face of an ICCD camera (Andor).

Ultraviolet hole-burning (UVHB) was employed to obtain the conformation specific electronic spectra of the individual conformers. UVHB is a double resonance technique, requiring the spatially overlapped output of two ultraviolet

lasers, temporally separated by 200 ns. The 10 Hz hole-burn laser is fixed on a transition due to a single conformer and preceded the 20 Hz probe, which is tuned through the region of interest. A difference spectrum is obtained by passing the integrated signal through a gated integrator operating in active baseline subtraction mode. Whenever the two lasers share the same ground state energy level, a depletion is observed.

Stimulated-emission pumping (SEP) ion-dip spectroscopy⁵¹ was performed in a molecular beam time-of-flight mass spectrometer and used to record the ^{12}C and ^{13}C ground state spectra between 800 and 900 cm^{-1} above the zero-point level of the *ttt* origin.⁵² Here, a 20 Hz UV pump laser was fixed on a UV transition due to a single conformation with a typical laser power of 0.1 mJ/pulse. The power was sufficient to excite the molecule to an electronic excited state, but produces a minimal amount of ion signal from resonant two-photon ionization. The second 20 Hz UV laser serves a dual purpose both as the second photon in 2C-R2PI and as the dump laser for SEP. The wavelength of this laser was tuned red of the origin with a laser power of 1.0 mJ/pulse to stimulate the emission back to the ground state in competition with ionization. Whenever the dump laser was resonant with a transition back to the ground state, a depletion in the total ion signal is observed. The technique provides analogous information to DFL, however, with a resolution predetermined by the laser linewidth. With mass selectivity, the technique is able to distinguish the spectra from ^{12}C and ^{13}C isotopomers even in the presence of spectral overlap.

Finally, the rotationally resolved electronic spectra were obtained at NIST by heating the sample to 135°C in a quartz nozzle with a $125\ \mu\text{m}$ diameter orifice. Details to the specific experimental apparatus have been reported previously.^{50,53} The molecules were entrained in an argon backing gas with a backing pressure of 0.2 bar. About 250 mW from an Ar^+ -pumped cw ring dye laser using C521 laser dye was frequency doubled in barium borate (BBO) in an external resonant cavity and the output mildly focused on a skimmed molecular beam 18 cm downstream of the source. The fluorescence was collected by two spherical mirrors and detected by a photomultiplier tube and photon counting system. Typical laser powers of 1–2 mW were used to record the rotationally resolved electronic spectra with a resolution of $\sim 21\text{ MHz}$.

III. COMPUTATIONAL METHODS

Excited state structural optimizations and vibrational frequency calculations for the *ttt* and *tgt* conformers of DPOE were performed using time-dependent density functional theory (TDDFT) at the M05-2X/6-31+G(d) level of theory. Rotationally resolved spectra were fit to an asymmetric rotor Hamiltonian using the genetic algorithm as implemented in the JB95 spectral fitting program.⁵⁴ The two optimized structures, *ttt* and *tgt*, were used as input for fitting the rotational spectra.

To better understand the excitonic splitting, the transition dipole coupling model (TDM) and the FG model have been employed.^{43,46} TDM is a simple electrostatic model in which the excitonic splitting is approximated utilizing the coulombic

interaction between the two electronic transition moments on the individual phenyl rings A and B. The interchromophore coupling is given by

$$V_{AB} = \frac{\mu_A \mu_B}{4\pi \epsilon R^3} (2 \cos \theta_A \cos \theta_B - \sin \theta_A \sin \theta_B \cos \varphi), \quad (1)$$

where μ is the magnitude of the electronic transition moment, R is the distance between the two transition moment vectors, θ is the angle between the two transition moment vectors along R , and φ is the dihedral between the two vectors.

The FG model for vibronic coupling uses a diabatic approach to model the vibronic structure observed in absorption and dispersed fluorescence.^{18,19} In earlier work,³⁴ we implemented a version of this model to explain the multi-mode vibronic coupling observed in bis-(4-hydroxyphenyl)methane. We use this same program to compare the model predictions with experiment in DPOE. Details of the model are given elsewhere.^{34,41}

IV. RESULTS

A. R2PI and dispersed fluorescence spectra

Figure 2 shows the 2C-R2PI spectrum (top trace) and the ultraviolet hole-burning spectra (bottom traces) of the two monomer conformations present in the supersonic jet expansion. 2C-R2PI was employed to avoid saturating the excitation spectrum. The small excursion from zero marked with an asterisk in the figure is present due to incomplete subtraction through the gated integrator when tuning through the *tgt* S_0 - S_1 origin. As discussed in the previous study reporting on the ground state preferences of DPOE,⁴⁷ the two isomers adopt geometries with C_2 and C_{2h} symmetry, differing exclusively by the central OCCO dihedral angle, *gauche* or *trans*. For this reason, the C_2 symmetric conformer has been labeled *tgt* and the C_{2h} isomer as *ttt* representing the *gauche* and *trans* isomers, respectively. The *tgt* origin occurs at $36\,423\text{ cm}^{-1}$ and the *ttt* origin at $36\,509\text{ cm}^{-1}$. The calculations predict an in-plane geometry of both Ph-O-C groups in both conformers, as is observed in alkoxy-benzenes such as 1,2-diethoxybenzene.⁵⁵

Given the C_2 symmetry of the *tgt* conformer A, calculations predict that transitions from S_0 to both the S_1 (A) and S_2 (B) electronic excited states will be dipole-allowed. The UVHB spectrum of the *tgt* conformer has several low-

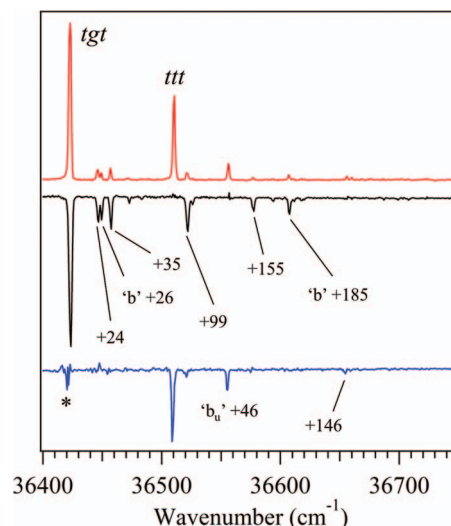


FIG. 2. 2C-R2PI and UVHB spectra of the two isomers present in the supersonic expansion. The asterisk marks an artifact due to incomplete subtraction through the gated integrator. Both UVHB spectra show vibronically induced fundamentals.

frequency vibronic transitions, including transitions $+24$, $+26$, $+35$, $+99$, $+155$, and $+185\text{ cm}^{-1}$ from the origin (Figure 2). Of these, the transitions at $+24$, $+35$, $+99$, and $+155\text{ cm}^{-1}$ are totally symmetric fundamentals with frequencies virtually unchanged from their values in the ground electronic state, as summarized in Table I. As an example, the DFL spectrum of the $+24\text{ cm}^{-1}$ band is shown in Figure 3(a). The spectrum is dominated by a false origin at -25 cm^{-1} , with vibronic structure built off this false origin closely similar to that of the electronic origin. The DFL spectra from the other totally symmetric fundamentals are similar, with false origins associated with X^1_1 transitions dominating the spectrum. These spectra are included in supplementary material.⁵⁹ The two remaining transitions at $+26\text{ cm}^{-1}$ and $+185\text{ cm}^{-1}$ are b symmetry fundamentals. Their DFL spectra are shown in Figure 3(a). These bands also display strong false origins in emission that confirm their assignments to “b” fundamentals with ground state frequencies of 30 and 186 cm^{-1} . Table I compares the observed ground and excited state frequencies of the *tgt* conformer with those predicted by calculation. The close correspondence confirms the assignments given. The “b” symmetry fundamentals appear in excitation as

TABLE I. A comparison of the calculated ground state vibrational frequencies to the experimental ground and excited state vibrational frequencies (in cm^{-1}) is presented. The Mulliken labeling scheme has been used for the normal modes.

C_2 (<i>tgt</i>)					C_{2h} (<i>ttt</i>)				
Mode #	Calc. frequency	Exp. S_0 freq	Exp. S_1 freq	Symmetry (mode)	Mode #	Calc. frequency	Exp. S_0 freq	Exp. S_1 freq	Symmetry (mode)
40	158	157	154	a	28 (R)	149	147	146	a_g
41	104	103	98	a	41	166			b_g
42	36	36	34	a	55	141			a_u
43	25	25	24	a	56	38			a_u
82	194	186	185	b	57	22			a_u
84	30	30	26	b	84 (\bar{R})	51	46	46	b_u

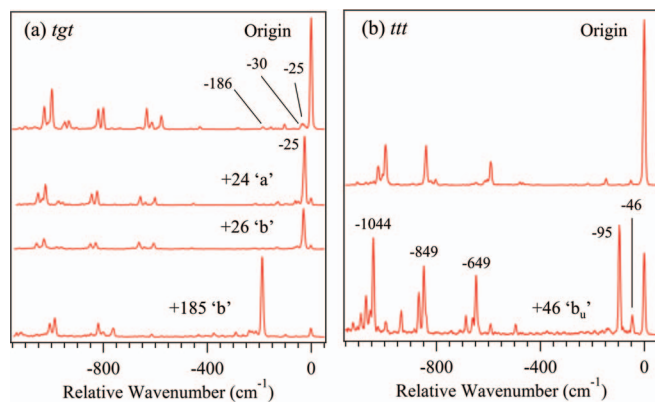


FIG. 3. Dispersed fluorescence spectra of the origin and key vibronic bands of (a) the *tgt* conformer and (b) the *ttt* conformer of DPOE.

a result of vibronic coupling between the S_1 and S_2 states. It is striking that all vibronic transitions are assigned to vibronic bands built off the single observed origin at $36\,423\text{ cm}^{-1}$. Thus, the location of the strong dipole-allowed S_0 – S_2 origin requires further investigation in what follows.

The C_{2h} symmetry *ttt* conformation has $S_1(A_g)$ and $S_2(B_u)$ electronic excited states with transitions from the ground electronic state $S_0(A_g)$ that are dipole forbidden and dipole-allowed, respectively. The UVHB spectrum of the *ttt* conformer is shown in the bottom trace of Figure 2. According to the calculations, the lowest frequency totally symmetric mode ($\nu_{28}(a_g)$, labeled R) in the C_{2h} *ttt* conformer is at 149 cm^{-1} , in reasonable agreement with the weak transition at $+146\text{ cm}^{-1}$ in the UVHB spectrum of the *ttt* isomer. The band 46 cm^{-1} above the B_u origin is assigned to a vibronically induced transition involving the lowest frequency b_u symmetry fundamental (ν_{84} , labeled \bar{R} here) with calculated ground state frequency of 46 cm^{-1} (Table I). Figure 4 presents the form of the R and \bar{R} vibrational modes, which involve symmetric and asymmetric in-plane bends of the two phenyl rings. It would appear built off the dipole-forbidden A_g symmetry excited state ($A_g X b_u$), gaining its oscillator strength completely through vibronic coupling. Its frequency position ($+46\text{ cm}^{-1}$) suggests that the dipole-forbidden origin must be near to the allowed A_g – B_u origin at $36\,509\text{ cm}^{-1}$.

The DFL spectra of the B_u electronic origin and $A_g(\bar{R}_0^1)$ transitions are presented for the *ttt* conformer in Figure 3(b). The origin emission spectrum has contributions only from a_g fundamentals, consistent with originating from a B_u excited electronic state. The $A_g(\bar{R}_0^1)$ band, however, has unusual vibronic activity, most notably in the triad of peaks observed at 0, -46 , and -95 cm^{-1} . The 0 and -95 cm^{-1} transitions

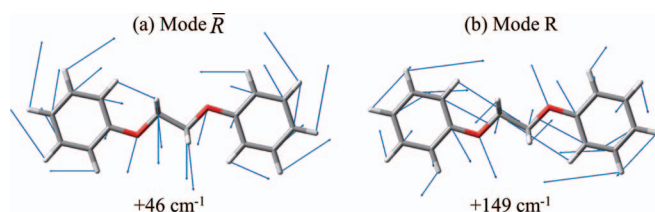


FIG. 4. Form of the normal modes of the *ttt* conformer of DPOE for the (a) b_u symmetry \bar{R} vibration (46 cm^{-1}) and (b) its a_g counterpart R (149 cm^{-1}).

are attributed to vibronic coupling, producing $\Delta\nu_{84} = \pm 1$ Herzberg-Teller selection rules. What is puzzling is the band at -46 cm^{-1} , which should only appear from an A_g symmetry vibronic level ($B_u X b_u$) in the excited state, since its ground state vibronic symmetry is $A_g X b_u = B_u$. Its DFL spectrum also shows increased intensity in several ring modes relative to the $B_u 0^0_0$ spectrum above it. The enhancement of ring mode intensity in emission was previously observed in the spectrum of the S_2 origin of bis-(4-hydroxyphenyl)methane³⁴ and attributed to vibronic coupling effects. In that case, the FG model was able to give a quantitative account of these intensity changes. We will present further analysis of this band using the FG model in Sec. V.

B. High resolution UV spectra

One intriguing possibility for the location of the S_0 – S_2 origin in the *tgt* conformer is that the electronic splitting is so small that it is unresolved from the S_0 – S_1 origin. Motivated by this notion, we recorded a high resolution UV spectrum ($\sim 21\text{ MHz}$ resolution) of the band at $36\,423\text{ cm}^{-1}$ assigned to the S_0 – S_1 origin. The resulting spectrum is presented in Figure 5(a) with the experimental spectrum as the top trace and the best fit produced by genetic algorithms as implemented in the JB95 spectral fitting program.⁵⁴ As hypothesized, the band is indeed composed of two transitions with band centers separated by 1.02 cm^{-1} . The two transitions are assigned to the S_0 – S_1 ($36\,422.91\text{ cm}^{-1}$) and S_0 – S_2 ($36\,423.93\text{ cm}^{-1}$) origins. The ground and excited state rotational constants and TDM directions are summarized in Table II. Note that the S_0 – S_1 transition is a 23:77 a:c-type band while the S_0 – S_2 origin is a pure b-type transition, with TDM directions that are perpendicular to one another. Furthermore, the excited state rotational constants of the two overlapped origin bands are remarkably similar to one another. Both these facts point to the electronic excitation being delocalized over the two rings, leading to geometry changes upon electronic excitation that are shared between the two rings, consistent with the C_2 geometry for the *tgt* conformer.

Figure 5(b) presents the high resolution spectrum of the S_0 – S_1 origin of the *ttt* conformer. Once again, the fit is shown

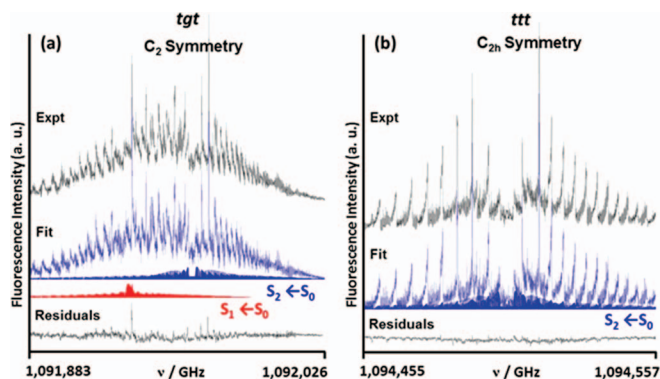


FIG. 5. High resolution LIF excitation spectrum of the electronic origin bands associated with the (a) *tgt* conformer and (b) *ttt* conformer. The fit to the experimental spectrum is shown in the bottom trace alongside the residuals to the fit.

TABLE II. The rotational constants for the two isomers of DPOE. The S_0 - S_1 origin of the *ttt* conformer is dipole-forbidden and therefore not observed. Rotational constants have been rounded for clarity (see Table S1 of the supplementary material⁵⁹ for a complete listing of fitted parameters including uncertainties).

		C_2 (<i>tgt</i>)		
	S_0 state (MHz)	S_1 state (MHz)	S_2 state (MHz)	
A	1873.8	ΔA	-66.4	-66.2
B	177.9	ΔB	0.9	0.8
C	171.1	ΔC	0.6	0.6
		24:76% a:c-type		100% b-type
		C_{2h} (<i>ttt</i>)		
A	2508.9	ΔA	...	-61.0
B	157.9	ΔB	...	-0.3
C	148.9	ΔC	...	-0.5
		100% b-type		

below for comparison, with best fit parameters shown in Table II. In this case, a single band is able to account for all observed rovibronic structure. The band is a b-type band, consistent with its assignment to the A_g - B_u transition of the C_{2h} *ttt* conformer. A high resolution scan of the $+46$ cm^{-1} transition of the *ttt* conformer is included in the supplementary material.⁵⁹ This transition is also of b-type, as anticipated based on the assignment of this transition to the b_u symmetry \bar{R} fundamental built off the A_g excited state. Given the close proximity of two electronic origins in the *ttt* conformer, and the position of the $+46$ cm^{-1} transition relative to its calculated frequency, it seems likely that the splitting between the A_g and B_u excited states should also be small. Proof for this conjecture comes in Sec. IV C.

C. ^{13}C -substituted R2PI spectroscopy

Following the lead of Leutwyler and co-workers,^{18,19,16} we recorded R2PI spectra of DPOE while monitoring the $M+1$ mass channel associated with incorporation of a single ^{13}C atom in the molecule, which contains 14 carbon atoms. Since 12 of the 14 carbons are in the two aromatic rings that typically give rise to similar electronic frequency shifts, the $M+1$ R2PI spectrum reflects primarily the effects of symmetry breaking on the electronic spectroscopy. These effects are anticipated to be particularly striking in the *ttt* conformer, since breaking the symmetry of the two rings can turn on intensity in the dipole-forbidden A_g - A_g electronic transition.

Figure 6 compares R2PI spectra recorded in the m/z 214 mass channel (all ^{12}C DPOE, top trace) to that in the $M+1$ mass channel, recorded under unsaturated (red, middle) and partially saturated (blue, bottom) conditions. The ^{13}C substitution in the ring produces a doublet at the *tgt* origin, split by 4.7 cm^{-1} , which is now resolved even under low resolution. The magnitude of this splitting is more than four times the excitonic splitting (1.02 cm^{-1}), indicating that most of the splitting in the ^{13}C spectrum is site splitting due to the fact that one ring contains a ^{13}C atom, while the other does not. On that basis, we surmise that the observed doublet should be

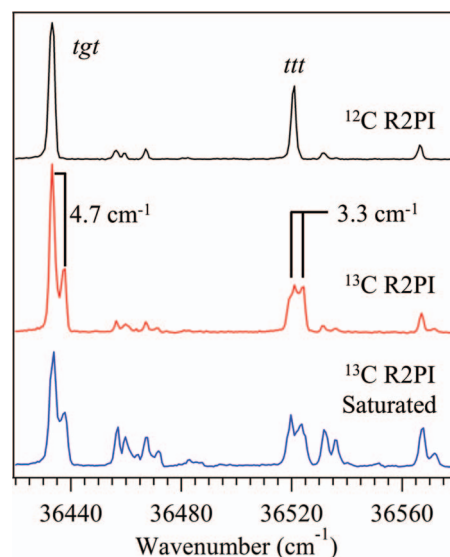


FIG. 6. R2PI spectra in the S_0 - S_1/S_2 origin regions of the *tgt* and *ttt* conformers of DPOE monitoring (a) the all ^{12}C parent mass channel, (b) the $M+1$ mass channel associated with incorporation of one ^{13}C into the molecule under (b) unsaturated and (c) partially saturated conditions. The observed splittings of 4.7 cm^{-1} and 3.3 cm^{-1} for the *tgt* and *ttt* conformations place upper bounds on the excitonic splittings of the two conformers. See text for further discussion.

interpreted as arising from electronic excitation largely localized on the all ^{12}C or singly ^{13}C substituted rings of DPOE.

Similar arguments hold for the R2PI spectrum of the ^{13}C *ttt* conformer. Here, we see a partially resolved and somewhat broadened doublet with a splitting of 3.3 cm^{-1} . Strikingly, the two transitions are nearly equal in intensity, as would occur if electronic excitation were completely localized on one or the other ring. This is consistent with a splitting of 3.3 cm^{-1} , which is 30% less than the splitting in the *tgt* conformer. We surmise on this basis that the splitting of the electronic origins in the all ^{12}C isotopomer is significantly smaller than 1 cm^{-1} for the *ttt* conformer. The partially saturated spectra show that the band splittings present at the origins carry forward to other vibronic bands in the spectrum.

D. Collisional studies

One important benefit of the ^{13}C R2PI spectrum is that it provides the electronic frequency positions of these transitions relative to the all- ^{12}C spectrum. In particular, the $+4$ cm^{-1} transition of the *ttt* conformer is directly overlapped with the main band of the ^{12}C spectrum, and would therefore be excited simultaneously under conditions for dispersed fluorescence. This raises the possibility that the -46 cm^{-1} transition in the *ttt* $+46$ cm^{-1} DFL spectrum (Figure 3(b)) could arise from the ^{13}C isotopomer, which would have an allowed transition with $\Delta v = 0$ Franck-Condon factors to the b_u fundamental in the ground electronic state. Indeed, its intensity relative to the $\Delta v = \pm 1$ transitions on either side of it, are approximately correct for ascribing the -46 cm^{-1} transition to ^{13}C DPOE.

It is noteworthy that the $+46$ cm^{-1} DFL spectrum shown in Figure 3(b) was recorded at $x/D = 38$, far downstream

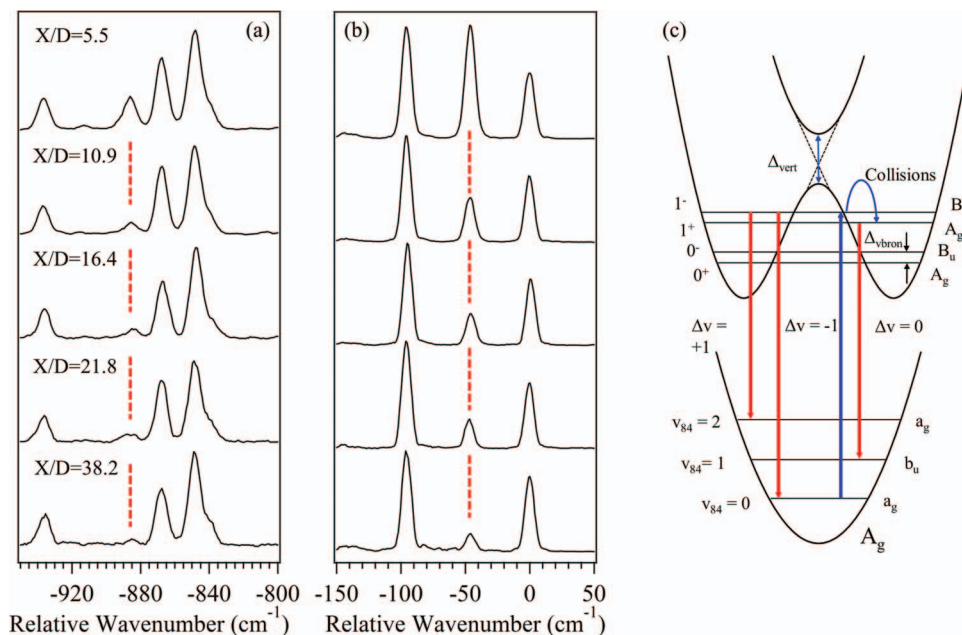


FIG. 7. Close-up views of the (a) -800 to -950 cm^{-1} and (b) $+50$ to -150 cm^{-1} regions of the ttt $+46$ cm^{-1} DFL spectrum taken with laser excitation occurring at different distances (x/D , D = nozzle diameter) from the nozzle in the expansion. Transitions marked with a dotted line grow in intensity at small x/D due to collisions with the backing gas. (c) Energy level diagram depicting the excitation, emission, and collisional energy transfer processes responsible for the collision free (0^+ -95 cm^{-1}) and collision-induced (-46 cm^{-1}) emission.

relative to conditions often used for recording DFL spectra. Under most circumstances, the effects of collisions on DFL spectra are minimal, since the collision frequency in the jet is typically slow relative to the excited state fluorescence lifetime (~ 30 ns in this case). However, the emission from the $+46$ cm^{-1} transition of ttt DPOE is a notable exception.

Figures 7(a) and 7(b) present a series of DFL spectra from the $+46$ cm^{-1} transition of ttt taken as a function of distances from the nozzle orifice (with diameter D), ranging from $x/D = 5.5$ to 38. A close-up of two regions of the DFL spectra are shown that highlight bands at -46 cm^{-1} and -889 cm^{-1} whose intensity is sensitive to the x/D position. Clearly, both bands grow in intensity by more than a factor of five as excitation occurs closer to the nozzle where collisions with buffer gas are more frequent.

Figure 7(c) displays an energy level diagram that summarizes the collisional mechanism responsible for the growth in this -46 cm^{-1} emission. The two excited states are drawn in an adiabatic representation in which the geometry changes accompanying electronic excitation of one or the other ring lead to displacements producing two equivalent, displaced wells in the excited state. The 1.02 cm^{-1} splitting between S_0-S_1 and S_0-S_2 origins is, in this adiabatic picture, a tunneling splitting associated with a process in which both electronic excitation and nuclear change accompany the tunneling. The $+46$ cm^{-1} transition in the excitation spectrum is to a B_u vibronic state that is (nominally) the b_u in-plane bending fundamental (\bar{R}) built off the A_g electronic origin ($A_g(\bar{R}_0^1)$). This state gains its oscillator strength by vibronic coupling with the B_u electronic state, and produces $\Delta v(\bar{R}) = \pm 1$ Herzberg-Teller selection rules in emission to produce transitions at 0^+ (resonance fluorescence) and -95 cm^{-1} (ending in $v = 2$ in the ground state). There is no dipole-allowed or vi-

bronically induced method of producing the $\Delta v = 0$ emission from this level to the corresponding $v = 1$ level (at -46 cm^{-1}) in the ground state. However, if collisions with buffer gas occur during the excited state lifetime (Figure 7(c)), they can produce the other member of the $v = 1$ tunneling doublet, which is less than 1 cm^{-1} away. This level is of $B_u x b_u = A_g$ vibronic symmetry, and has a dipole-allowed transition to the $v = 1$ level in the ground state, with emission frequency -46 cm^{-1} from resonance fluorescence, as observed.

Interestingly, even at $x/D = 38$, some intensity remains in the -46 and -896 cm^{-1} bands. Although the remaining intensity could be attributed to collisions with an extremely large cross section for the collisional energy transfer process, it seemed more likely to us that this residual intensity arises from overlap with the ^{13}C 0^0_0+46 cm^{-1} transition (Sec. III C). As a final test of this conjecture, we recorded SEP ion-dip spectra from the ttt $+46$ cm^{-1} intermediate state while monitoring the ^{13}C and all ^{12}C mass channels. The results are shown in Figure 8.

Unfortunately, since the SEP “dump” laser frequency at -46 cm^{-1} was near resonances in absorption for the tgt conformer, the SEP ion-dip spectrum could not be recorded in the region of Figure 7(b) where the -46 cm^{-1} transition occurs. Instead, the corresponding collision-induced band at -889 cm^{-1} (Figure 7(a)) was free from such interference. As Figure 8 shows, the transition at -889 cm^{-1} is clearly observed in the ^{13}C spectrum, but is completely absent in the ^{12}C spectrum, confirming that the ^{13}C isotopomer is the likely source of the remaining -46 cm^{-1} intensity in Figures 3(b) and 7(b). This transition is dipole-allowed in the ^{13}C spectrum due to localization of the electronic excitation induced by one ring possessing a ^{13}C atom.

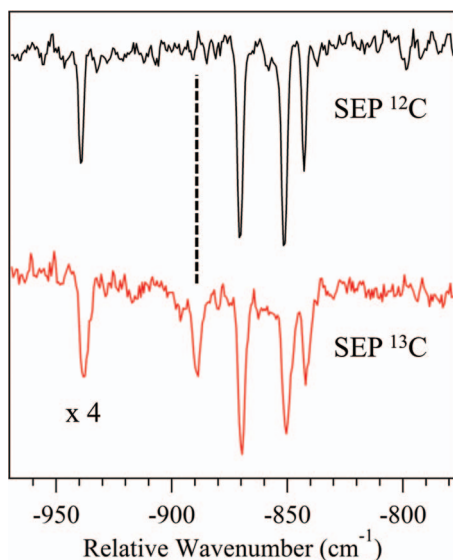


FIG. 8. The ^{12}C and ^{13}C stimulated emission pumping spectra indicating the 889 cm^{-1} transition is due to the ^{13}C spectrum.

V. DISCUSSION

A. The weak vibronic coupling limit

The primary goal of the present study has been to map out in some detail the conformational dependence of the excited state surfaces present in the model flexible bichromophore DPOE. In earlier work, LIF excitation, UV-hole burning, and resonant ion-dip infrared spectra were used to observe and assign transitions due to two conformations, the *ttt* conformer of C_{2h} symmetry, and the *tgt* conformer, with C_2 symmetry. In this paper, we have determined the magnitude of the excitonic splitting between the S_1 and S_2 states for both conformers, and determined and analyzed the spectroscopic signatures of vibronic coupling between the S_1 and S_2 states in the two conformations.

Perhaps the most striking result of this work is the extraordinarily small excitonic splittings present in the two conformers, with the *tgt* conformer possessing a splitting of

1.02 cm^{-1} , and its *ttt* counterpart even smaller based on the spectrum of its isotopomer containing a single ^{13}C atom in one of the rings. This is to be compared with an electronic transition from S_0 of more than $34\,000\text{ cm}^{-1}$. Thus, DPOE is in the extreme limit of weak vibronic coupling, with an excitonic splitting similar in size to the recently studied benzoic acid dimer (0.94 cm^{-1}).⁴⁵

The splittings of the exciton coupled S_1 and S_2 origins reported in previous jet-cooled studies of the C_2 symmetric bichromophores, bis-(4-hydroxyphenyl)methane,³⁴ and diphenylmethane³³ were in excess of 100 cm^{-1} because of the close proximity of the two chromophores. In these cases, both exciton states are orbitally allowed and the vibronic spectra built off of each origin are readily resolved. The close proximity of the two rings rotates the direction of each ring's TDM and induced an out-of-ring-plane TDM component, significantly increasing the excitonic coupling relative to a monomer point-dipole model.³⁵ In contrast, the chromophores of DPOE are more weakly coupled because of the larger inter-ring separations that minimize direct interactions between the rings.

The weak coupling in DPOE is evident from predictions for the exciton splitting based on the transition dipole coupling of Förster theory,¹⁰ and from vertical splittings calculated at the TDDFT M05-2X/6-31+G(d) level of theory. These are summarized in Table III for DPOE. The TDDFT vertical splittings (9 cm^{-1} for *tgt*, 25 cm^{-1} for *ttt*) and transition dipole coupling estimates (17 cm^{-1} for *tgt*, 43 cm^{-1} for *ttt*) are generally consistent with one another, and are quite small compared to those in DPM and b4HPM. For the *ttt* isomer of DPOE, the distance between the center-of-masses of the two aromatic rings is 8.6 \AA , while in *tgt* this distance is 8.0 \AA . Yet, these estimates are still more than 10-fold too large compared to the experimental splittings between the S_0 - S_1 and S_0 - S_2 origins (1 cm^{-1} or less).

Within the diabatic model typically used for analysis of excitonic splitting, the vertical splitting (Δ_{elec}) is vibrationally “quenched” by a Franck-Condon factor that accounts for the shift in excited state geometry relative to the ground state minimum.¹⁶ This leads in the weak vibronic coupling limit to a “quenched” vibronic splitting Δ_{vibron} that is more than

TABLE III. Calculated vertical frequencies, S_1/S_2 splittings and oscillator strengths at the TDDFT M05-2X/6-31+G(d) level of theory. Comparison with experimental splittings and the excitonic splittings predicted with the transition dipole coupling model (TDM).

		Conformer: <i>tgt</i>		
	Vertical splitting (cm^{-1})	Scaled vertical splitting (cm^{-1})	Exp. freq (cm^{-1})	Calc. osc. strength
S_0 - S_1	43 617	36 422.91	36 422.91	0.0277
S_0 - S_2	43 628	36 432.09	36 423.93	0.0440
	TDDFT splitting	9 cm^{-1}	Exp. splitting	
	TDM splitting	17 cm^{-1}	1.02 cm^{-1}	
		Conformer: <i>ttt</i>		
	Vertical splitting (cm^{-1})	Scaled vertical splitting (cm^{-1})	Exp. freq (cm^{-1})	Calc. osc. strength
S_0 - S_1	43 737	36 523.12	...	0.0000
S_0 - S_2	43 767	36 548.17	36 508.77	0.0683
	TDDFT splitting	25 cm^{-1}	Exp. splitting	
	TDM splitting	43 cm^{-1}	$\sim 1.0\text{ cm}^{-1}$	

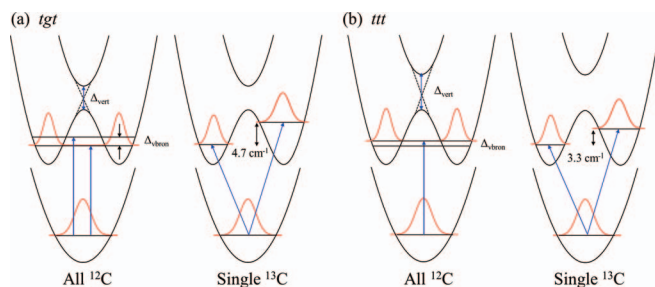


FIG. 9. Schematic adiabatic potential energy curves for the (a) *tgt* and (b) *ttt* conformers of DPOE showing (left) electronic delocalization of the symmetric all ^{12}C structures with tunneling splittings of $\Delta_{\text{vibron}} = 1.02$ and $\sim 1 \text{ cm}^{-1}$, respectively, and (right) the electronic localization associated with incorporation of a single ^{13}C atom into one of the rings, with S_1/S_2 splittings of 4.7 and 3.3 cm^{-1} , respectively.

10-fold smaller, with experimental splittings of 1.02 cm^{-1} (*tgt*) or less (*ttt*).

In this circumstance, the observed splitting is understood most intuitively in an adiabatic model in which the observed splitting is considered as a nonadiabatic tunneling splitting on the lower double-minimum potential energy surface. This is shown schematically for the two conformers of DPOE in Figure 9. As Kopec *et al.*¹⁶ have laid out in some detail, this tunneling splitting cannot be calculated from the shape of the lower double minimum surface alone, since the tunneling is influenced by nonadiabatic interactions with the upper electronic state.

At the same time, the rotational constants and TDM orientations extracted from the rotationally resolved spectra provide unequivocal evidence that the electronic excitation is completely delocalized over the two aromatic rings, with TDM directions consistent with excited states which are equal contributions from local excitations of anisole ($\text{C}_6\text{H}_5\text{OCH}_3$). In the end, this is a requirement of the symmetric configurations for the two conformers, in which the two aromatic chromophores are placed in equivalent configurations.

On this basis, one would anticipate that most other geometries that are away from these highly symmetric points on the excited state potential energy surfaces will be characterized by nearly localized electronic excitation of the two rings with even modest shifts of a few cm^{-1} in the site frequencies sufficient to cause electronic localization, since the nonadiabatic tunneling splittings at C_2 and C_{2h} geometries are 1 cm^{-1} or less. This fact was brought home in dramatic fashion by the R2PI spectra of the singly ^{13}C -substituted isotopomer of DPOE, where shifts in the zero-point energies of the two excited states of $3\text{--}4 \text{ cm}^{-1}$ led to substantial localization of the electronic excitation, as Figure 9 illustrates. In the *ttt* conformer, this turned a pair of electronic transitions in which one is dipole-allowed and the other dipole-forbidden into a pair of transitions that have nearly equal oscillator strengths, with excitation localized either on the ^{13}C -substituted ring or the non-substituted one, with a splitting of 3.3 cm^{-1} . One could imagine that, in the condensed phase, small asymmetries or fluctuations in the solvent surroundings will be sufficient to localize electronic excitation there too. The effects of asym-

metric solvation are seen already in the DPOE– H_2O complex involving the asymmetry induced by a single H_2O molecule.⁵⁶

B. Spectroscopic signatures of vibronic coupling involving near-degenerate excited states

We have just proven that in both the *tgt* and *ttt* conformers of DPOE, the first two levels on the adiabatic double-minimum potential energy surface, associated with electronic character

$$\begin{aligned}\psi_1 &= \frac{1}{\sqrt{2}}(|A^*B\rangle + |AB^*\rangle), \\ \psi_2 &= \frac{1}{\sqrt{2}}(|A^*B\rangle - |AB^*\rangle),\end{aligned}\quad (2)$$

are separated in energy by no more than 1 cm^{-1} at the C_2 and C_{2h} geometries associated with the *tgt* and *ttt* conformers, respectively. This splitting is small compared to all vibrational frequencies in the *tgt* and *ttt* conformers. As a result, each vibrational level is split by nonadiabatic effects into a pair of levels. We focus in this section on the spectroscopic signatures of this near-degeneracy in the vibronic spectroscopy of the two conformers.

In the C_2 *tgt* conformer, both members of the tunneling doublet associated with each vibronic level carry oscillator strength from S_0 . As a result, every vibronic transition in the *tgt* spectrum in Figure 2 is in fact an unresolved doublet, as was shown in Figure 5 to be the case at the electronic origin by high resolution spectroscopy. Furthermore, the strong intensities observed in the non-totally symmetric fundamentals result from vibronic coupling between the two states, with the S_1 state borrowing intensity from S_2 and vice versa. Since the emission from both members of the pair is dipole-allowed, a strong $\Delta v = 0$ false origin appears in the DFL spectra of both totally symmetric and non-totally symmetric fundamentals (Figure 3(a)).

By contrast, the C_{2h} *ttt* conformer has only one dipole-allowed electronic transition ($A_g\text{--}B_u$), but ^{13}C R2PI spectra located the dipole-forbidden $A_g\text{--}A_g$ origin split by only 3.3 cm^{-1} . Based on a comparison with the *tgt*, where a 4.7 cm^{-1} ^{13}C splitting arose from a 1.02 cm^{-1} non-adiabatic tunneling splitting, the two states are placed within 1 cm^{-1} of one another. As a result, once again, each vibronic band is split into a pair of transitions, but in this case only one member of each pair carries intensity. Vibronic coupling nevertheless plays an important role in the spectrum, with the band 46 cm^{-1} above the $A_g\text{--}B_u$ origin assigned to b_u symmetry \bar{R} fundamental built off the A_g electronic state, gaining its intensity purely through vibronic coupling.

It is worth noting that the smaller splitting ascribed to the *ttt* conformer is opposite to the ordering of the splittings predicted by TDM model or TDDFT calculations (Table III). One possible reason for this smaller splitting would be that the *ttt* conformer has a larger Franck-Condon quenching than *tgt*. However, comparison of the DFL spectra of the S_1 origins of *ttt* (Figure 3(b)) and *tgt* conformers (Figure 3(a)) show little difference between the two in the intensities of the ring modes that dominate this quenching factor. In the end, the

only experimentally measured quantity we report here for the *ttt* conformer is the 3.3 cm^{-1} splitting in the ^{13}C R2PI spectrum, which is the composite of the quenched excitonic and zero-point energy effects that include contributions from the different sets of inter-ring modes for each conformer given in Table I. A direct measure of the splitting in the ^{12}C isotopomer would require comparison of the one-photon and two-photon allowed transitions, a task left for future work.

The adiabatic model developed by Kopec *et al.*¹⁶ projects non-adiabatic coupling onto a single effective vibrational coordinate, leading to accurate predictions for the nonadiabatic tunneling splitting at the electronic origin in model homodimers. By contrast, a multi-mode version of the diabatic Fulton-Gouterman model has recently been developed, providing a means for modeling the observed vibronic intensities in DPOE. The *tgt* conformer was not modeled due to the unresolved overlap of contributions from the two excited states in the excitation and dispersed fluorescence spectra. In the *ttt* conformer, the model is able to account for the vibronic intensities in the R/\bar{R} pair of interchromophore bends both in excitation and in dispersed fluorescence from the dipole-allowed B_u origin (Fig. S1 of the supplementary material⁵⁹). Similar modeling of the intensities in the origin emission into the ring mode pairs 6a, 1, and 12 (in Varsanyi notation)⁵⁷ at $-590/-610$, $-802/-840$, and $-996/-1005\text{ cm}^{-1}$ are similarly successful (Figs. S2–S4 of the supplementary material⁵⁹). Similar modeling of the $A_g(\bar{R}^1)$ emission (the $+46\text{ cm}^{-1}$ band) accounts for the vibronically induced emission to $v'' = 0, 2$. However, the strong emission bands from the $A_g(\bar{R}^1)$ level to transitions at -649 , -849 , and -1044 cm^{-1} are not accounted for in the FG model, pointing to the need for further refinement of intermode coupling in the theory.

C. Collision-induced electronic energy transfer

One of the more striking results of the present study is the unusual sensitivity of the DFL spectrum of the *ttt* $+46\text{ cm}^{-1}$ band to collisions, as shown in Figures 7(a) and 7(b). As discussed in some detail in Sec. IV D and shown pictorially in Figure 7(c), we have shown that the bands that grow in can be ascribed to the lower member of the non-adiabatic tunneling doublet associated with the R^1_0 fundamental. This state is dipole forbidden from the S_0 zero-point level, but its close proximity (within 1 cm^{-1}) to the other member of the tunneling doublet initially populated by the laser provides a pathway for collisional energy transfer that is extremely facile, and competes with fluorescence even under conditions under which one would typically have thought were collision-free.

Table IV presents estimates of the number of collisions experienced by DPOE during the lifetime of the excited state (30 ns), assuming a gas-kinetic cross section for transfer between members of the tunneling doublet ($\sigma_{\text{coll}} = 75\text{ \AA}^2$). Under conditions closest to the nozzle, there are multiple collisions during the excited state lifetime, suggesting that the two tunneling states could have their populations equilibrated. On the other hand, at $x/D = 38$, where only 1% of the excited state molecules undergo a gas-kinetic collision, the remaining intensity is likely to be mostly or entirely due to the ^{13}C

TABLE IV. Fractional collision-induced intensity in the $\Delta v_{84} = 0$ transition of the *ttt* conformer of DPOE relative to that in the $\Delta v_{84} = \pm 1$ transitions as a function of distance from the nozzle in nozzle diameters, x/D . The number of gas-kinetic collisions experienced by DPOE in its excited state lifetime is given for comparison.

x/D	No. of collisions ^a	Fractional collision induced intensity
5	2.15	0.56
11	0.32	0.17
16	0.11	0.08
22	0.05	0.05
38	0.01	0.00 ^b

^a Assuming a gas-kinetic collision cross section of 75 \AA^2 . Calculated using the equations of Ref. 49, 58

^b By assumption. See text for further discussion.

isotopomer. Invoking these assumptions, the intensity ratio on the right of the table is the collision-induced intensity in the -46 cm^{-1} band relative to the sum of the “0” and -95 cm^{-1} transitions. This ratio falls off at a rate in keeping with the fall off in number of collisions. While these data are not sufficient to quantify the magnitude of the collision cross section as a function of position in the expansion, it seems likely to us that very large cross sections for electronic energy transfer across this small tunneling doublet are at play, with glancing collisions with cross sections significantly exceeding gas kinetic are possible.

It is interesting to consider how these studies under jet-cooled conditions in the gas phase transfer into condensed phase environments in which collisions are likely to provide an efficient means of interchromophore electronic energy transfer in chromophore arrays, multichromophore polymers, and the like.

VI. CONCLUSIONS

We have presented detailed spectroscopic data on the close-lying S_1/S_2 states of DPOE that prove that the molecule is in the extreme limit of weak vibronic coupling. At the C_2 and C_{2h} geometries, the electronic excitation is delocalized over the two rings (by symmetry), but the splitting between the two states is 1 cm^{-1} or less. Given this weak coupling, it is likely that the two potential energy surfaces lie within a few cm^{-1} of one another over large regions of the torsional potential energy surface. In this weak vibronic coupling limit, the excitonic splitting is best thought of as a nonadiabatic tunneling splitting on the lower double-minimum potential energy surfaces associated with electronic excitation on one or the other aromatic ring. This splitting is more than a factor of 10 smaller than vertical splittings calculated via standard methods. In light of this weak vibronic coupling, the smallest of perturbations to one of the rings is sufficient to localize the electronic excitation on one or the other ring. This was illustrated in dramatic fashion in the spectra recorded for the ^{13}C isotopomer that contains a single ^{13}C atom somewhere in one or the two aromatic rings. This zero-point asymmetry was enough to split the electronic origins by 4.7 cm^{-1} (*tgt*) and 3.3 cm^{-1} (*ttt*), and nearly completely localize the electronic

excitation. One would anticipate similar effects by asymmetric solvation in the condensed phase. We will show elsewhere the interesting effects associated with binding a single H₂O molecule to DPOE.⁵⁶

ACKNOWLEDGMENTS

E.G.B., P.S.W., and T.S.Z. gratefully acknowledge support from the (U.S.) Department of Energy (DOE) Basic Energy Sciences, Division of Chemical Sciences under Grant No. DE-FG02-96ER14656.

- ¹G. Panitchayangkoon, D. V. Voronine, D. Abramavicius, J. R. Caram, N. H. C. Lewis, S. Mukamel, and G. S. Engel, *Proc. Natl. Acad. Sci. U.S.A.* **108**, 20908 (2011).
- ²K. M. Pelzer, G. B. Griffin, S. K. Gray, and G. S. Engel, *J. Chem. Phys.* **136**, 164508 (2012).
- ³G. S. Engel, T. R. Calhoun, E. L. Read, T. K. Ahn, T. Mancal, Y. C. Cheng, R. E. Blankenship, and G. R. Fleming, *Nature (London)* **446**, 782 (2007).
- ⁴H. Lee, Y. C. Cheng, and G. R. Fleming, *Science* **316**, 1462 (2007).
- ⁵S. Polyutov, O. Kuhn, and T. Pullerits, *Chem. Phys.* **394**, 21 (2012).
- ⁶R. Tempelaar, A. Stradomska, J. Knoester, and F. C. Spano, *J. Phys. Chem. B* **117**, 457 (2013).
- ⁷S. Habuchi, H. Fujita, T. Michinobu, and M. Vacha, *J. Phys. Chem. B* **115**, 14404 (2011).
- ⁸O. R. Tozer and W. Barford, *J. Phys. Chem. A* **116**, 10310 (2012).
- ⁹M. Maus, R. De, M. Lor, T. Weil, S. Mitra, U. M. Wiesler, A. Herrmann, J. Hofkens, T. Vösch, K. Mullen, and F. C. De Schryver, *J. Am. Chem. Soc.* **123**, 7668 (2001).
- ¹⁰G. D. Scholes, *Annu. Rev. Phys. Chem.* **54**, 57 (2003).
- ¹¹J. D. Hybl, A. A. Ferro, and D. M. Jonas, *J. Chem. Phys.* **115**, 6606 (2001).
- ¹²D. M. Jonas, *Annu. Rev. Phys. Chem.* **54**, 425 (2003).
- ¹³F. Fassioli, A. Olaya-Castro, and G. D. Scholes, *J. Phys. Chem. Lett.* **3**, 3136 (2012).
- ¹⁴H. Hossein-Nejad, A. Olaya-Castro, and G. D. Scholes, *J. Chem. Phys.* **136**, 024112 (2012).
- ¹⁵D. R. Borst, J. R. Roscioli, D. W. Pratt, G. M. Florio, T. S. Zwier, A. Müller, and S. Leutwyler, *Chem. Phys.* **283**, 341 (2002).
- ¹⁶S. Kopec, P. Ottiger, S. Leutwyler, and H. Koppel, *J. Chem. Phys.* **137**, 184312 (2012).
- ¹⁷A. Müller, F. Talbot, and S. Leutwyler, *J. Chem. Phys.* **116**, 2836 (2002).
- ¹⁸P. Ottiger, S. Leutwyler, and H. Koppel, *J. Chem. Phys.* **131**, 204308 (2009).
- ¹⁹P. Ottiger, S. Leutwyler, and H. Koppel, *J. Chem. Phys.* **136**, 174308 (2012).
- ²⁰K. Le Barbu-Debus, M. Broquier, F. Lahmani, and A. Zehnacker-Rentien, *Mol. Phys.* **103**, 1655 (2005).
- ²¹N. Seurre, K. Le Barbu-Debus, F. Lahmani, A. Zehnacker-Rentien, and J. Sepiol, *Chem. Phys.* **295**, 21 (2003).
- ²²C. A. Southern, D. H. Levy, J. A. Stearns, G. M. Florio, A. Longarte, and T. S. Zwier, *J. Phys. Chem. A* **108**, 4599 (2004).
- ²³C. G. Heid, P. Ottiger, R. Leist, and S. Leutwyler, *J. Chem. Phys.* **135**, 154311 (2011).
- ²⁴M. Chattoraj, B. Paulson, Y. Shi, G. L. Closs, and D. H. Levy, *J. Phys. Chem.* **97**, 13046 (1993).
- ²⁵W. T. Yip, D. H. Levy, R. Kobetic, and P. Piotrowiak, *J. Phys. Chem. A* **103**, 10 (1999).
- ²⁶N. A. van Dantzig, D. H. Levy, C. Vigo, and P. Piotrowiak, *J. Chem. Phys.* **103**, 4894 (1995).
- ²⁷X. Wang, D. H. Levy, M. B. Rubin, and S. Speiser, *J. Phys. Chem. A* **104**, 6558 (2000).
- ²⁸A. Zehnacker, F. Lahmani, E. Breheret, J. P. Desvergne, H. Bouas-Laurent, A. Germain, V. Brenner, and P. Millie, *Chem. Phys.* **208**, 243 (1996).
- ²⁹A. Zehnacker, F. Lahmani, J. P. Desvergne, and H. Bouas-Laurent, *Chem. Phys. Lett.* **293**, 357 (1998).
- ³⁰A. L. L. East, P. Cid-Aguero, H. S. Liu, R. H. Judge, and E. C. Lim, *J. Phys. Chem. A* **104**, 1456 (2000).
- ³¹J. K. Lee, R. H. Judge, B. H. Boo, and E. C. Lim, *J. Chem. Phys.* **116**, 8809 (2002).
- ³²N. R. Pillsbury, C. W. Muller, W. L. Meerts, D. F. Plusquellic, and T. S. Zwier, *J. Phys. Chem. A* **113**, 5000 (2009).
- ³³N. R. Pillsbury, J. A. Stearns, C. W. Muller, D. F. Plusquellic, and T. S. Zwier, *J. Chem. Phys.* **129**, 114301 (2008).
- ³⁴C. P. Rodrigo, C. W. Mueller, N. R. Pillsbury, W. H. James III, D. F. Plusquellic, and T. S. Zwier, *J. Chem. Phys.* **134**, 164312 (2011).
- ³⁵J. A. Stearns, N. R. Pillsbury, K. O. Douglass, C. W. Muller, T. S. Zwier, and D. F. Plusquellic, *J. Chem. Phys.* **129**, 224305 (2008).
- ³⁶Y. Inokuchi, O. V. Boyarkin, R. Kusaka, T. Haino, T. Ebata, and T. R. Rizzo, *J. Am. Chem. Soc.* **133**, 12256 (2011).
- ³⁷S. Kokubu, R. Kusaka, Y. Inokuchi, T. Haino, and T. Ebata, *Phys. Chem. Chem. Phys.* **12**, 3559 (2010).
- ³⁸R. Kusaka, Y. Inokuchi, and T. Ebata, *Phys. Chem. Chem. Phys.* **10**, 6238 (2008).
- ³⁹N. A. van Dantzig, H. S. Shou, J. C. Alfano, N. C. C. Yang, and D. H. Levy, *J. Chem. Phys.* **100**, 7068 (1994).
- ⁴⁰E. E. Baquero, W. H. James III, T. H. Choi, K. D. Jordan, and T. S. Zwier, *J. Phys. Chem. A* **112**, 11115 (2008).
- ⁴¹B. Nebgen, F. L. Emmert, and L. V. Slipchenko, *J. Chem. Phys.* **137**, 084112 (2012).
- ⁴²T. Forster, in *Modern Quantum Chemistry*, edited by O. Sinanoglu (Academic, New York, 1965), p. 93.
- ⁴³R. L. Fulton and M. Gouterman, *J. Chem. Phys.* **35**, 1059 (1961).
- ⁴⁴R. L. Fulton and M. Gouterman, *J. Chem. Phys.* **41**, 2280 (1964).
- ⁴⁵P. Ottiger and S. Leutwyler, *J. Chem. Phys.* **137**, 204303 (2012).
- ⁴⁶R. L. Fulton and M. Gouterman, *Spectrochim. Acta* **17**, 1093 (1961).
- ⁴⁷E. G. Buchanan, E. L. Sibert, and T. S. Zwier, *J. Phys. Chem. A* **117**, 2800 (2013).
- ⁴⁸T. S. Zwier, *J. Phys. Chem. A* **105**, 8827 (2001).
- ⁴⁹T. S. Zwier, *J. Phys. Chem. A* **110**, 4133 (2006).
- ⁵⁰W. Majewski and W. L. Meerts, *J. Mol. Spectrosc.* **104**, 271 (1984).
- ⁵¹R. J. Stanley and A. W. Castleman, *J. Chem. Phys.* **94**, 7744 (1991).
- ⁵²J. R. Clarkson, E. Baquero, V. A. Shubert, E. M. Myshakin, K. D. Jordan, and T. S. Zwier, *Science* **307**, 1443 (2005).
- ⁵³D. F. Plusquellic, S. R. Davis, and F. Jahanmir, *J. Chem. Phys.* **115**, 225 (2001).
- ⁵⁴D. F. Plusquellic, jpb95 - spectral fitting program, NIST, Gaithersburg, MD, 2009, see <http://physics.nist.gov/jpb95>.
- ⁵⁵V. A. Shubert, W. H. James, and T. S. Zwier, *J. Phys. Chem. A* **113**, 8055 (2009).
- ⁵⁶E. G. Buchanan, J. R. Gord, and T. S. Zwier, *J. Phys. Chem. Lett.* **4**, 1644 (2013).
- ⁵⁷G. Varsanyi, *Assignments for Vibrational Spectra of 700 Benzene Derivatives* (Wiley, New York, 1974).
- ⁵⁸D. M. Lubman, C. T. Rettner, and R. N. Zare, *J. Phys. Chem.* **86**, 1129 (1982).
- ⁵⁹See supplementary material at <http://dx.doi.org/10.1063/1.4807300> for dispersed fluorescence spectra of the totally symmetric fundamentals for the *tgt* conformer, details, and results specific to using the multi-mode Fulton-Gouterman model of vibronic coupling on the *ttt* isomer, the principal axis orientation of both conformers, and a table listing the parameters and uncertainties from the genetic algorithm and linear least-squares fits of the origin bands of DPOE are provided for clarity.